ORIGINAL PAPER

Drug delivery system based on PVA and clay for potential treatment of COVID-19

Mirela Teodorescu[1] (ORCID) · **Simona Morariu**[1]

Abstract

Tremendous efforts are being made around the world to develop efficient ways to prevent/treat the novel β-coronavirus disease (COVID-19) caused by SARS-CoV-2. There are currently many studies and clinical trials (either based on computational predictions or clinical experiences), in progress, focusing on finding relevant protein targets and medications anti-COVID-19. In the present study, we report a hydrogel drug delivery system based on Laponite® RD (Lap) entrapped in a poly(vinyl alcohol) (PVA) matrix obtained by freezing/thawing method. The PVA/Lap hydrogels were characterized in terms of their morphological, rheological, and swelling properties. Moreover, in vitro drug delivery investigations were performed with a promising drug, Rifampicin (Rif). Rif is an antitubercular drug and was selected for this study in order to demonstrate its efficacy as an anti-COVID-19 repurposed drug. In vitro studies were supplemented by in silico molecular docking simulations of Rif capacity of inhibition against SARS-CoV-2 target protein 3-chymotrypsin-like protease (3CL^{pro}). The results obtained in this study are encouraging and we propose the Rif loaded PVA/Lap hydrogels as promising drug delivery systems for COVID-19 treatment, promoting a synergistic therapeutic effect by dual targeting of viral 3CL^{pro} and S proteins.

Keywords Drug delivery system · Laponite® RD · Poly(vinyl alcohol) · Rifampicin · 3-chymotrypsin-like protease · Coronavirus

Introduction

We are currently in the midst of the third type of coronavirus-induced pandemic of the last two decades, after SARS and MERS outbreaks in 2002 and 2012, respectively. Although SARS was contained by drastic public health measures in 2003, it caused an alarmingly high mortality rate of 10% [1]. Ten years later, the world was confronted with the second coronavirus pandemic (i.e., MERS), which registered an even higher fatality rate of about 36%, and despite the efforts of the scientific community to discover specific drugs, this pandemic has not been eradicated to date [2]. In the context of the current global health crisis caused by COVID-19, multiple pathways have been tackled for more than two years to urgently develop efficient and safe methods to prevent/treat the infection with SARS-CoV-2.

These pathways are generally based on one of the following strategies: classic development of antiviral drugs/vaccines, convalescent plasma transfusion or drug repurposing [3, 4]. However, the classic approach of drug discovery is a time consuming process, which takes about 10 to 15 years, implies high costs and has a very low rate of success. Moreover, the treatment with antibodies from convalescent patients was observed to cause side effects, sometimes leading to adverse reactions of the immune system or even increasing the viral infectivity [5]. Drug repurposing, which consists in identification of possible new disease targets for previously certified medications outside their original therapeutic application, seems to be an attractive option and certainly the fastest method.

During the last two years, many studies have been focused on identifying possible drug repurposing for COVID-19, using virtual screening of already marketed FDA approved drugs [6]. As a result, some antiviral drugs which were previously used for treating Ebola, malaria, HIV/AIDS, SARS, and MERS have already been included in multiple clinical trials and also in treating SARS-CoV-2 infected patients [7].

✉ Mirela Teodorescu
  teodorescu.mirela@icmpp.ro

1 "Petru Poni" Institute of Macromolecular Chemistry, 41-A Grigore Ghica Voda Alley, 700487 Iasi, Romania

There are thousands of therapeutic compounds (both natural and synthetic) examined by molecular docking studies and some of them present promising perspectives, triggered by their high level of binding affinity to viruses. However, in order to develop appropriate treatment strategies in fighting against this new coronavirus-induced disease, there should be followed important steps in understanding virus genomic structure, as well as infection mechanisms. These aspects have been discussed in detail in a recently published review [8]. Only after these steps are thoroughly completed, we can expect efficient design of antiviral targeted therapies and vaccines.

The discovery of an efficient therapeutic compound might be based on one of the following approaches: (i) inhibiting the functional proteins and enzymes, vital for virus survival; (ii) inhibiting viral structural proteins, blocking the interaction with host cells and virion assembly; (iii) inhibiting human proteins acting as receptors for virus; (iv) immunity stimulation.

The structure of SARS-CoV-2 is composed of several structural and non-structural proteins, which might be candidate druggable targets [9]. For example, spike (S) proteins facilitate virus binding with angiotensin-converting enzyme 2 (ACE2) receptors of human target cells and mediate virus entry [10]. Blocking S protein binding with ACE2 receptors is an attractive strategy to fight SARS-CoV-2 infection and has been previously reported in developing therapeutic antibodies against SARS [11]. However, the treatment of SARS-CoV infection with antibodies was sometimes associated with unwanted side effects [5]. Therefore, attention has been focused on the identification of natural compounds that have been proved safe for human consumption, and use them as potential treatment for COVID-19. Among these natural compounds, clays have been used in medical purposes for ages and were also proved to be efficient in treating some coronaviruses due to their capacity to bind with the viral S proteins, thus prohibiting virus attachment and entering the target cell. Clay minerals present very high level of affinity for bacteria and viruses, also against several coronaviruses and rotaviruses [10, 12]. In this context, a recent study based on molecular simulation proposes nano-clays (e.g., montmorillonite) to act like pseudo-antibodies, predicting that clays may be efficient blockers and inhibitors of SARS-CoV-2 entry into the human cells, by targeting the receptor-binding domain (RBD) of S protein before the virus binding to human ACE2 receptors [10]. Another versatile clay with promising perspectives in developing various systems for medical field, also for COVID-19 prevention and treatment, is Laponite® RD (Lap). Lap belongs to the smectite clays, which are characterized by a 2:1 type layered structure favourable to absorption of microorganisms [13]. Moreover, by incorporating Lap into a polymeric matrix, there could be obtained different materials (e.g., nanofibers, films, hydrogels, etc.), with enhanced properties, as drug delivery systems, tissue engineering scaffolds, wound dressings, etc. Among the polymers used, poly(vinyl alcohol) (PVA) is a well-known polymer highly employed in medical applications, due to its biocompatibility, biodegradability, good mechanical properties, and adhesivity. In this context, PVA has been proved to be a promising candidate for biomedical and pharmaceutical applications [14, 15]. For example, hydrogels based on Lap and PVA have been proposed as wound healing dressings, due to their interesting properties, such as: high surface roughness and swelling degree, large elasticity, good transparency, and flexibility [16, 17]. In another study, the presence of Lap into a PVA hydrogel-based drug delivery system, loaded with Rifampicin (Rif), led to an increase of the antibacterial activity against gram-positive and gram-negative bacteria [17].

Another potential target for drug discovery is 3-chymotrypsin-like protease (3CL^{pro}), also known as main protease. Because 3CL^{pro} has a highly conserved structure among SARS, MERS and SARS-CoV-2, it might help in developing pan-coronavirus new protease inhibitors. Among the vast range of therapeutic compounds examined, that might target the 3CL^{pro} of SARS-CoV-2, Rif appeared to be by far the most promising drug against COVID-19 in some recently published studies [18–21]. The molecular docking analysis revealed that the drug Rif presents high binding affinity to 3CL^{pro} active site, in some cases being considerably better than other drugs used on a large scale for COVID-19 treatment, such as: Lopinavir, Ritonavir, Chloroquine, Hydroxychloroquine, Indinavir, Azithromycin, etc. [18–21].

Due to these promising results, the present study proposes a step forward into developing a drug delivery system by dual targeting of 3CL^{pro} and S protein, through enclosing Rif in a PVA/Lap hydrogel. Based on previous reported studies and on our findings, we premise that the presented drug delivery system might be promising for mitigating COVID-19 and promoting a synergistic therapeutic effect.

Experimental part

Materials

Lap was provided by BYK Additives Ltd. (Widnes, U.K.). Lap is a synthetic clay with the formula Na$_{0.70}$[(Si$_8$Mg$_{5.5}$Li$_{0.3}$)O$_{20}$(OH)$_4$], which belongs to the 2:1 phyllosilicates. PVA (98–99% hydrolysed) was purchased from LOBA Feinchemie AG (Austria Chemical Companies). The viscometric molecular weight (M_v) of PVA was determined as being $9.6 \cdot 10^4$ g·mol^{-1}, by using the following Mark–Houwink equation [22]:
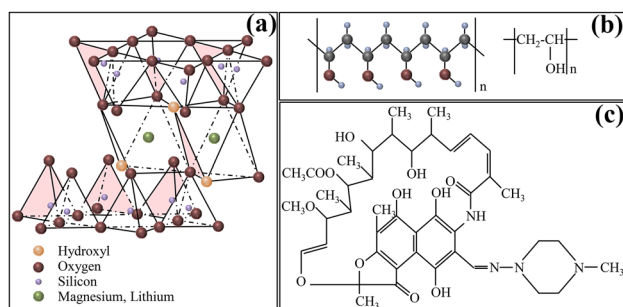
Fig. 1 Chemical structure of: (**a**) Laponite® RD, (**b**) Poly(vinyl alcohol), and (**c**) Rifampicin

$$[\eta] = 4.28 \cdot 10^{-4} \cdot M_v^{0.64} (dL \cdot g^{-1}) \tag{1}$$

The intrinsic viscosity ($[\eta]$) was determined in water, at 30 °C, with the Huggins equation:

$$\frac{\eta_{sp}}{c} = [\eta] + k_H \cdot [\eta]^2 \cdot c \tag{2}$$

where: η_{sp}/c, k_H and c represent the reduced viscosity, Huggins constant and polymer concentration, respectively.

The drug Rif was kindly donated by S.C. Antibiotice S.A. Iasi, Romania.

All materials were used without any further purification. The chemical structures of Lap, PVA, and Rif are presented in Fig. 1.

Synthesis of hydrogels

PVA solutions with the concentrations (c_{PVA}) of 2%, 4% and 6.2% were prepared by dissolving the polymer in deionized water, at 80 °C, under vigorous stirring for 8 h and resting overnight at room temperature. For the preparation of hydrogels containing clay, only half content of polymer

solutions was used and, in each of them, an amount of 0.5% Lap dispersion (c_{Lap}) was added to obtain clay/polymer ratio presented in Table 1. The obtained dispersions were stirred for 1 h, at room temperature, and then were subjected to five freezing/thawing (F/T) cycles in liquid nitrogen (freezing for 5 min and 4 h thawing at ambient temperature). The samples were dried by freeze-drying method, in a Martin Christ ALPHA 1-2LD lyophilizer, for 2 days. The samples were denoted as P_X and P_X-C (where P, C and X represent the polymer (PVA), the clay (Lap) and the polymer concentration in solutions subjected to F/T cycles, respectively). For drug release investigation, P_4-C and $P_{6.2}$-C hydrogels in presence/absence of Lap were loaded with 3% Rif calculated against polymer content. Rif was added to polymer/clay dispersions, which were then subjected to five F/T cycles. The concentrations are expressed as weight percentage (wt%).

Scanning electron microscopy

The morphology of hydrogels was determined by using a scanning electron microscope (SEM) type Quanta 200 (operating voltage of 20 kV). SEM measurements were performed on the cross-section of the lyophilized hydrogels. ImageJ and OriginPro8 software were used to estimate the pores size and their distribution histograms, respectively. P_2 and P_2-C gels were too crumbly in lyophilized state and their SEM investigation was not possible.

Rheological measurements

The measurements for establishing the rheological properties were carried out at 25 °C, by using a MCR 302 Anton-Paar rheometer (plane-plane geometry, diameter of 25 mm). The temperature control was provided by a Peltier device and, in order to limit the water evaporation, a solvent trap cover was used. The amplitude sweep tests were performed at an

Table 1 Composition, viscoelastic and swelling parameters of investigated samples

Sample	Lap/PVA (g/g)	τ_l^a (Pa)	γ_l^a (%)	τ_c^a (Pa)	E_c^b (J·m^{-3})	n^c	k^c (min^{-n})	DR^d (%)	mass loss^d (%)
P_2	0	1.9	6.7	9.1	698	-	-	-	-
P_2-C	0.25	15.1	6.4	32.3	5193	-	-	-	-
P_4	0	7.4	4.8	80.7	1767	0.17	0.65	98.9	34.4
P_4-C	0.12	4.8	6.7	43.6	3097	0.12	0.43	79.7	18.9
$P_{6.2}$	0	-	-	-	-	0.28	0.37	81.7	24
$P_{6.2}$-C	0.08	-	-	-	-	0.28	0.26	82.5	12.7

$^a\tau_l$ and γ_l represent the limiting shear stress and strain, respectively, and τ_c is the critical shear stress, which were determined from LVR

^bE_c is the cohesive energy calculated with Eq. 4

^{c}n and k are the power law coefficient and the kinetic constant, respectively, from Korsmeyer-Peppas equation (Eq. 5)

^{d}DR is percentage of drug released, and mass loss represents PVA and Lap mass from hydrogel released at the same time with the drug

oscillatory frequency (ω) of 10 rad·s^{-1} and shear stress (τ) between 10^{-2} Pa and $2 \cdot 10^2$ Pa, in order to determine the linear viscoelastic regime (LVR) of hydrogels. The frequency sweep measurements were performed from 10^{-1} rad·s^{-1} to 10^2 rad·s^{-1} at 1 Pa (within the linear viscoelastic regime). For the P$_{6.2}$ and P$_{6.2}$-C samples, the rheological measurements were not possible due to their brittleness.

Swelling experiments

The swelling degree, S, of PVA/Lap hydrogels in water was determined at room temperature. S was calculated with the following relationship:

$$S = \frac{m_t - m_o}{m_o} \cdot 100 \qquad (3)$$

where m_o is the weight of the dried hydrogel and m_t represents the hydrogel weight at the immersion time t.

After the immersion in water, the samples were gently wiped out with an absorbent paper, before their weighing. Three swelling measurements were performed for each sample and an average value of S was calculated. The standard deviations of the swelling degrees were represented in the swelling degree – immersion time graph.

In vitro drug delivery

The known amounts of lyophilized samples containing Rif were immersed in 10 mL MilliQ water, at 37 °C, in a shaker incubator (100 rpm). 1 mL of solution was withdrawn from the release medium at different times. This solution was filtered through a 0.20-μm cellulose acetate filter and absorbance was determined at 475 nm with a JENWAY-650 UV–VIS Spectrophotometer (Jenway, UK). By using the recorded absorbance values, the released drug concentration (expressed in mg·mL^{-1}) was calculated considering the slope and the intercept of the calibration curve determined previously. The measurements were performed two times and the average value was considered.

In silico study of drug efficacy

Molecular docking method

Molecular docking is a frequently used computational simulation method that can predict the preferred binding orientation of a small molecule ligand and a target protein with which it forms a stable complex. Thus, it is a valuable and reliable tool for fast and cost-effective drug design/repurposing. Molecular docking simulation was performed by using AutoDock 4.2 software, and the free energy (ΔG) binding

of the complex formed by SARS-CoV-2 3CL^{pro} with Rif was determined.

Selection of ligand/drug

Antitubercular drug Rif was recommended as potential coronavirus inhibitor by various recently published papers [18–21]. Thus, Rif was selected for molecular docking with SARS-CoV-2 3CL^{pro}. The file of three-dimensional chemical structure of the FDA approved Rif drug was selected from PubChem database of NCBI (https://pubchem.ncbi.nlm.nih.gov/), downloaded in structure data file (SDF) format, and further used for molecular docking.

Selection and preparation of target protein

The 3CL^{pro} of SARS-CoV-2 was used as a target protein for Rif, supposing that key residues of amino acids present in its binding pocket might form hydrogen bonds with the selected drug. The file of 3D X-ray crystal structure of 3CL^{pro}, complexed with an inhibitor N3 (N-[(5-methylisoxazol-3-yl)carbonyl]alanyl-l-valyl-n ~ 1 ~ -((1R,2Z)-4-(benzyloxy)-4-oxo-1-{[(3R0-2—oxopyrrolidin-3-yl]methyl}but-2-enyl)-l-leucinamide), was downloaded in PDB format from Protein Data Bank (PDB ID: 6LU7) [23]. The 3CL^{pro} has two chains A and B, but only the chain A was subjected to ligand binding simulation. Discovery Studio software was used to prepare the target 3CL^{pro} protein for docking, by removing all water molecules and the ligand N3 (attached to the protein binding site), which was used as a control molecule. Further, AutoDock Tools software was used to assign Kollman charges and add hydrogen atoms (polar only). The grid box covering all the amino acids of interest present in the protein active site was defined considering the number of grid points in each dimension as $60 \times 60 \times 60$, with the grid spacing of 0.375 Å. The coordinates of central grid point were: x = -9.768, y = 11.436, and z = 68.904, respectively. The stochastic Lamarckian genetic algorithm was selected for computing ligand (Rif) poses/conformations. At the same time, the thermodynamic stability of the complex, formed by the ligand docked inside the binding pocket of target protein, is estimated by optimizing scoring function. AutoDock simulation was run 100 times in Cygwin, after which the results were examined.

Results and discussions

PVA/Lap hydrogels with different amounts of polymer in presence/absence of Lap (Table 1) were prepared by F/T method. The effect of PVA concentration on the morphology,

viscoelastic properties and swelling degree of the obtained hydrogels were investigated and discussed.

Hydrogels morphology

Figure 2 exemplifies the cross-sectional morphology of PVA/Lap hydrogels in presence/absence of clay.

P_4 and P_4-C hydrogels presented sponge-like structures in which the pores are not well-defined (Fig. 2a,b). The mean values of pores sizes for P_4 and P_4-C samples were 17.38 μm

and 13.08 μm, respectively. The maximum size of pores for both samples was about 25 μm and 36 μm, respectively, with the higher value for the sample free of clay. The standard deviation (S.D.) of pore size distribution decreases from 7.54 for P_4 to 4.75 for P_4-C.

The increase of PVA concentration causes a better outline of the pores formed in the hydrogel (Fig. 2a compared with 2c). Moreover, the $P_{6.2}$ hydrogel presented large pores, with the average diameter of about 29.80 μm (Fig. 2c). The addition of Lap determined the decrease of the average pore
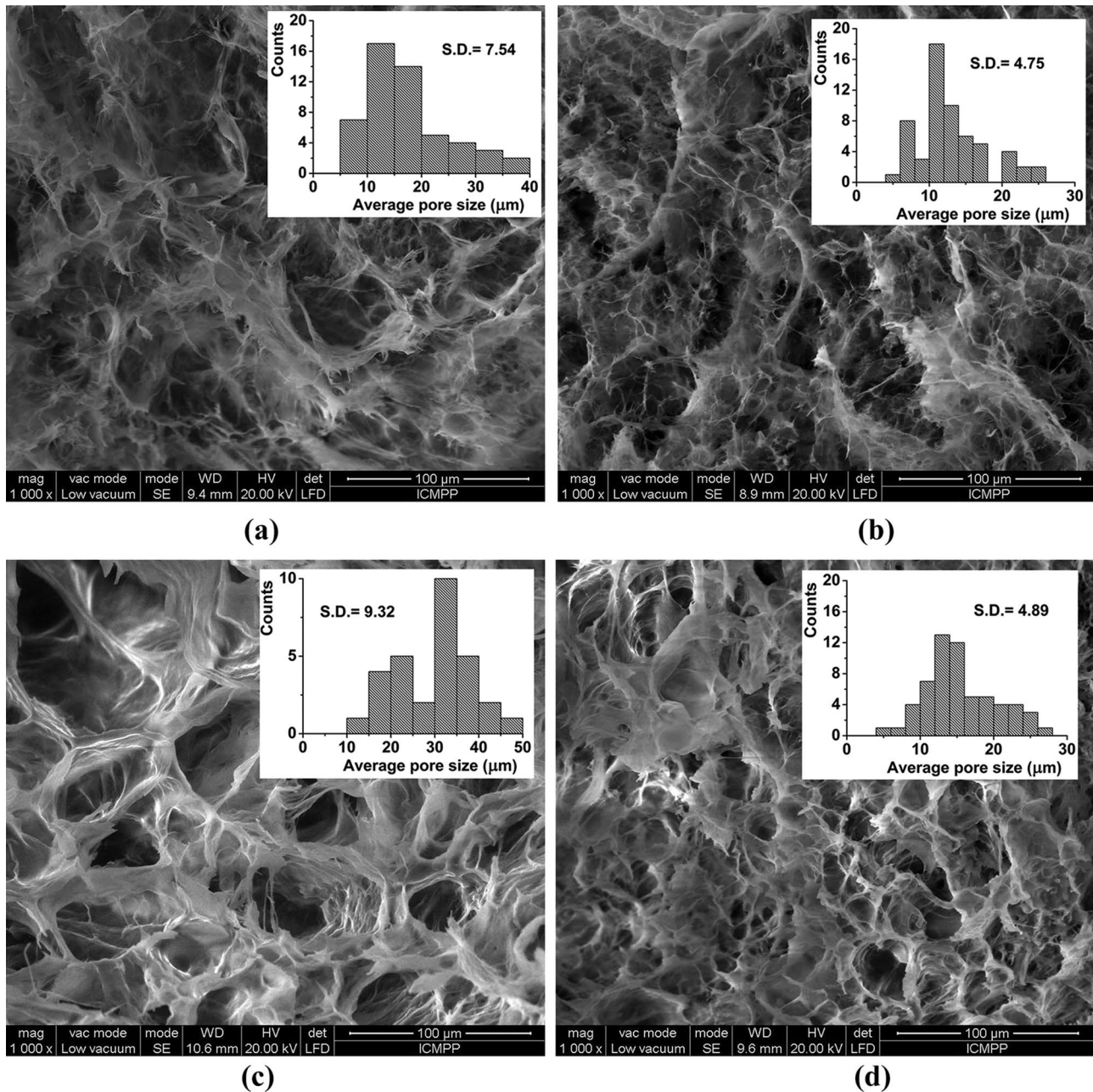

Fig. 2 SEM micrographs of (**a**) P_4, (**b**) P_4-C, (**c**) $P_{6.2}$ and (**d**) $P_{6.2}$-C. The insets represent the mean pore size distribution and the values of standard deviation (S.D.)

diameter to 12.66 μm. The adsorption of PVA chains on the clay discs surface causes the formation of a physical network with small holes in which the ice nuclei are formed during the F/T cycle, leading to the decrease of the formed pores size (Fig. 2d). The S.D. value of $P_{6.2}$-C hydrogel pores decreases by the addition of clay from 9.32 to 4.89. The lower S.D. value for $P_{6.2}$-C proves that the clay particles were uniformly distributed through the PVA chains in 6.2% PVA solution subjected to F/T, leading to a hydrogel with pores close in size. These results are in accordance with our previous findings [17], were we proved that at low Lap concentrations the clay particles are distributed uniformly in the polymer matrix, while at higher clay concentrations some large Lap aggregates are formed. Regardless of PVA concentration, the addition of clay causes the decrease of the S.D value.

Rheological properties

All samples, independent of PVA concentration and content of Lap, revealed a gel-like behaviour, with storage modulus (G′) greater than loss modulus (G″) (Fig. 3).

In terms of PVA amount influence on the viscoelastic moduli, Fig. 3 reveals that higher polymer content (P_4 hydrogel, Fig. 3b) leads to increased G′ and G″ values (compared with P_2 hydrogel, Fig. 3a). This might be explained by the formation of a PVA network with higher crosslinking density. The addition of clay causes the increase of viscoelastic moduli for the sample with 2% PVA (Fig. 3a). Namely, G′ and G″ values of the P_2-C hydrogel increase with an order of magnitude, as compared

with P_2 sample. For the hydrogel having higher PVA amount, the addition of Lap determines a slight increase of G″, while G′ value does not change significantly (P_4 and P_4-C samples, Fig. 3b). In the PVA solutions with low polymer concentration (i.e., 2%), the mobility of polymer chains and clay particles is high, favouring the formation of both polymer–polymer interactions and polymer–clay interactions which lead to improved rheological parameters. By increasing the concentration of PVA, the adsorption of polymer chains on the clay particles surface to create new polymer–clay interactions is prevented and the polymer–polymer interactions become more favourable. The addition of a small amount of Lap into the PVA solution with high polymer concentration does not determine the formation of a high number of polymer–clay or clay-polymer–clay interactions. The rheological behaviour is mainly determined by the interactions established between the polymer chains.

Viscoelastic moduli, G′ and G″, are constant up to a limit shear stress (τ_1) (see Fig. 3a) from which the hydrogel structure starts to change and the structural breakdown occurs [24]. The limiting shear stress, which corresponds to a limiting strain (γ_1), increases as the hydrogel network becomes stronger. By further increasing the τ, the sample acquires liquid-like properties (G′ < G″), at a shear stress value corresponding to a critical shear stress, τ_c. τ_1 and τ_c values, as well as those of corresponding γ_1, are shown in Table 1. τ_1 increases from 1.9 Pa for P_2 to 15.1 Pa for P_2-C. In contrast, LVR of the samples with 4% PVA decreases slightly by the addition of clay (from 7.4 Pa for P_4 to 4.8 Pa for P_4-C).
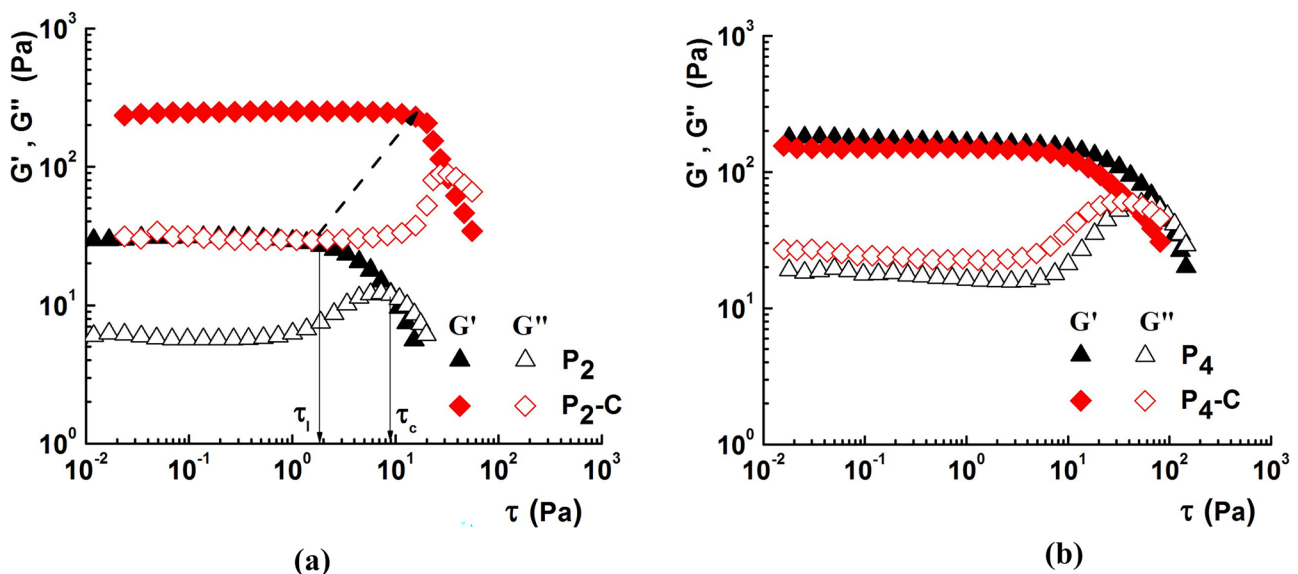

Fig. 3 Evolution of the viscoelastic moduli, G′ and G″, as a function of shear stress, τ, at 10 rad·s^{-1} for (**a**) P_2 and P_2-C and (**b**) P_4 and P_4-C hydrogels, at 25 °C

The energy necessary to break the hydrogel network is given by the cohesive energy (E_c). E_c can be calculated with the following equation [25]:

$$E_c = \frac{1}{2} G_o \gamma_l^2 \tag{4}$$

where γ_l is the limiting strain from which the hydrogel shows a non-linear viscoelastic behaviour and G_0 represents the elastic modulus in linear region.

P_2 sample exhibits the lowest cohesive energy as a result of the weak strength of the polymer network. For both PVA concentrations (2% and 4%), the addition of Lap determines the increase of E_c as a result of the intensification of polymer–polymer interactions and the formation of additional polymer–clay interactions. The most stable network was observed for the P_2-C and the weakest network was of the P_2 sample.

The gel-like properties (G′ higher than G″) of the investigated hydrogels without or with Lap were also evidenced by frequency sweep tests performed from 10^{-1} rad·s^{-1} to 10^2 rad·s^{-1} at a shear stress from LVR (Figs. 4a,b). For all samples, the interactions (polymer–polymer and/or polymer–clay) responsible for the network formation are not very affected during shearing and G′ value is nearly constant over the frequency range explored. G″ value is dependent of ω showing an increase (more accentuated for samples with 2% PVA) after an oscillatory frequency value which depends on the sample composition. Thereby, G″ values of the samples with 2% PVA and 4% PVA start to increase from about 0.4 Pa and 10 Pa, respectively. This behaviour of G″ is typical for soft materials characterized by structural disorder and metastability [26]. Such materials

present a very high energy barrier (compared with typical thermal energies), which is not enough for complete structural relaxation and the systems adopt a disordered and metastable configuration.

As observed for the samples analysed by SEM, the decrease of PVA concentration causes a decrease of the pores average size and a random distribution of them in the network structure. In addition, for samples with 2% PVA, the density of the network is lower and the amount of polymer and/or clay particles not trapped in the network is high. The structural characteristics of samples P_2 and P_2-C favour the dissipation of energy during rheological testing leading to an increase of G″ at higher oscillatory frequencies.

Swelling measurements

The hydrogels swelling in water was studied over a period of approximately six hours and the diffusion mechanism was discussed considering the Korsmeyer-Peppas model [27]:

$$\frac{M_t}{M_\infty} = k \cdot t^n, for \, M_t/M_\infty < 0.60 \tag{5}$$

where M_t is the water amount absorbed at time t, M_∞ is the mass of water absorbed at equilibrium, k (min^{-n}) is the kinetic constant, while n is the power law coefficient showing the type of diffusion mechanism of water molecules.

In Fig. 5a is illustrated the variation of the swelling degree, S, as a function of the immersion time in water for the hydrogels containing 2% PVA and 4% PVA. The n and k values determined from the representation of $log(M_t/M_\infty)$ as a function of $log \, t$ (Fig. 5b) are given in Table 1. As can
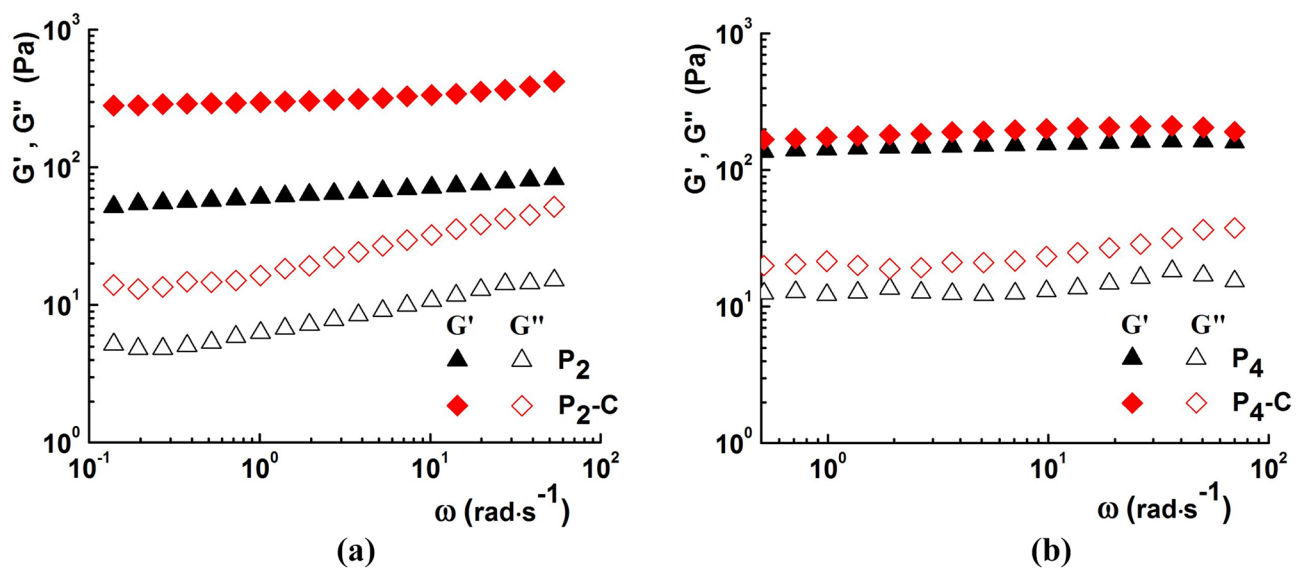

Fig. 4 Variation of G′ and G″, as a function of oscillatory frequency, ω, for (**a**) P_2 and P_2-C and (**b**) P_4 and P_4-C hydrogels at 25 °C and 1 Pa

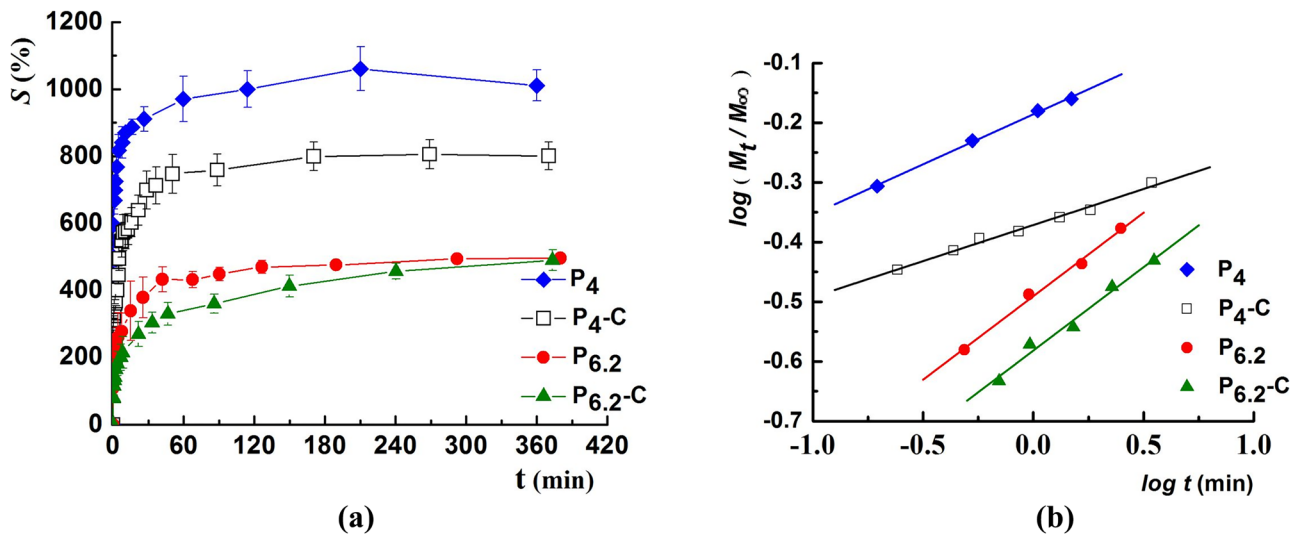**Fig. 5** (**a**) The swelling degree (*S*) as a function of the immersion time in water, at room temperature, and (**b**) the plots of $log(M_t/M_\infty)$ as a function of $log\ t$ for hydrogels containing 4% and 6.2% PVA, respectively. Error bars represent the average values $\pm$ standard deviation

be seen, all values for *n* are lower than 0.45. This shows that the diffusion of water molecules into the hydrogel network is pseudo-Fickian, which is characterized by quick absorption of water in the initial phase and then slowly reaching the equilibrium value. The *k* values are bigger for smaller polymer concentrations, which indicate that the diffusion speed is higher at these concentrations. This might be explained by the lower crosslinking density of the hydrogel network. By increasing the polymer concentration, the swelling degree drops, due to the formation of a denser hydrogel. Thus, high water amount is prohibited to enter into its structure. Moreover, when clay is added, the swelling degree is further decreasing and a more pronounced decrease is observed for hydrogels with smaller polymer concentration (i.e., P_4-C). This swelling behaviour of hydrogels can also be observed in Fig. 5a, where P_4 and P_4-C samples absorb 970% and 750% water, respectively, in the first 60 min of immersion, while $P_{6.2}$ and $P_{6.2}$-C absorb only approximately 470% and 338% water, respectively.

Drug release

The proposed drug Rif was used due to its promising results reported by in silico studies as a good inhibitor for 3CL^{pro} [18–21]. It is a semisynthetic broad spectrum antibiotic (against gram-positive and gram-negative organisms), obtained from Streptomyces mediterranei, and is known to inhibit the activity of bacterial DNA-dependent RNA polymerase, with which forms a stable drug-enzyme complex, thus suppressing the initiation of RNA synthesis [28]. However, Rif does not inhibit human RNA polymerase. Although it is generally used in tuberculosis treatment, it gave good

results in treating MERS-CoV infected patients [29], as well as some rare cases of polyinfection (tuberculosis, HIV and COVID-19) [30]. Rif has a macrocyclic amide structure as presented in Fig. 1.

The influence of polymer concentration on the in vitro release kinetics of Rif was investigated for hydrogels with/without clay. The information offered by the drug supplier mention that Rif solubility in water is influenced both by temperature and pH. Thus, at 25 °C and pH = 7.3, the drug solubility in water is 2.5 mg·mL^{-1}, while for 37 °C and pH = 7.4 and pH = 8, the solubility values are 3.35 mg·mL^{-1} and 5.44 mg·mL^{-1}, respectively [31]. In order to not exceed the limit concentration from which Rif is insoluble at 37 °C and basic pH, only an amount of 1 mg·mL^{-1} of drug was used in the initial polymer/clay dispersions, subsequently subjected to F/T process. Moreover, the clay addition into the hydrogels might favourably influence the solubility of Rif, as well as tuning its release profile/time [32]. In Fig. 6 is exemplified the Rif release profile from some of the hydrogels with/without clay.

The percentage of drug released (*DR*) was given by the following relation:

$$DR = \frac{Q_t}{Q_i} \cdot 100\ \%$$ (6)

where Q_t is the quantity of drug released at time *t* and Q_i is the initial Rif amount loaded in the hydrogels.

It was observed that the largest amount of drug released, over a period of approximately 90 min, is 98.9% for hydrogels with a lower concentration of PVA (i.e., the P_4 sample). For hydrogels with a higher polymer concentration (i.e., the $P_{6.2}$ sample), the amount of drug released drops at 81.7%.

This may be explained by the formation of a hydrogel with a denser structure, in which PVA binds the drug molecules by various physical interactions and prevents them from being released. The clay addition affects differently the release of the drug depending on the PVA concentration. Thus, for the P_4-C hydrogel, the presence of clay causes a decrease in the amount of drug released to 79.7%, probably due to the occurrence of drug-clay interactions that retain the drug in the hydrogel. Together with the drug, a certain amount of polymer and clay is released into the water. Thus, P_4 and $P_{6.2}$ hydrogels free of clay show a mass loss of 34.4% and 24%, respectively (Table 1). By adding clay, the weight loss decreases to 18.9% for P_4 and 12.7% for $P_{6.2}$. The decrease of the mass lost is due on the one hand to the development of new polymer–clay interactions, and on the other hand to the additional interactions established between Rif molecules and clay particles.

The larger value of the standard deviation of the sample P_4 obtained for *DR* (Fig. 6) and *S* (Fig. 5a) could be correlated with its SEM micrographs which show a non-homogenous structure with pores not very well-defined.

Generally, the mechanical properties of hydrogels used for drug delivery purposes strongly depend on their route of administration. Thus, they should present a convenient mechanical integrity so that to remain intact within the different body environments, until they reach and deliver the drugs at the targeted site. However, the literature does not show clearly the correlation between drug release properties of hydrogels and their mechanical properties. The main rheological properties for drug delivery hydrogels refer to their elasticity and strength, between which an optimum ratio should be obtained. The hydrogel elasticity contributes to proper circulation of the drug within the polymeric matrix, while an adequate strength can be tuned, for example, by
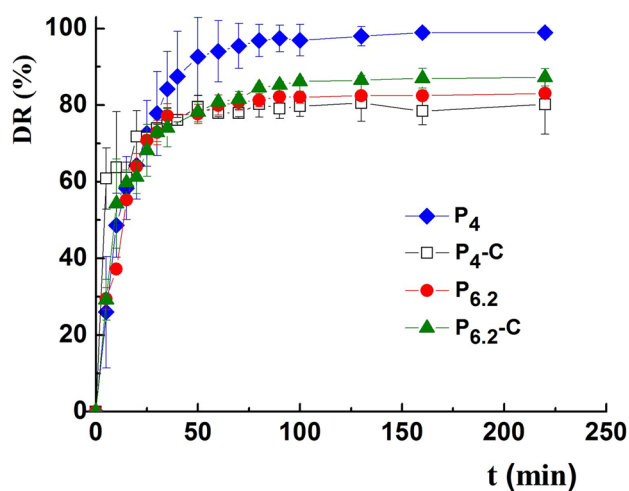

Fig. 6 Rifampicin release profile from the investigated hydrogels. Error bars represent average values ± standard deviation

varying the crosslinking degree or by incorporating different fillers. In light of our findings and taking into consideration both rheological parameters, obtained for the investigated samples and the percentage of released drug, we can conclude that the sample P_4-C would be the most viable for application as drug delivery hydrogel.

Discussion on Rif and clay influence on SARS-CoV-2 3CL[pro] and S proteins

After SARS-CoV-2 enters the target cell its replication starts by RNA translation into two long overlapping polyproteins (i.e., pp1a and pp1ab). These polyproteins are fragmented by two cysteine proteases (i.e., 3CL[pro] and PL[pro]), thus releasing the proteins needed for viral assembly. The X-ray crystal structure of SARS-CoV-2 3CL[pro] has been reported in early 2020 by Jin et al. [23], and has been the starting point for multiple molecular docking studies to develop anti-COVID-19 drugs based on protease inhibitors. 3CL[pro] crystal structure (Fig. 7) reveals that the protease has a homodimeric structure composed of two 306-residue protomers, chain A and chain B (Fig. 7a). Each of these protomers has three domains (I, II, and III) (Fig. 7b). The enzymatic activity of 3CL[pro] is played by the dyad of residues Cys 145 – His 41(Fig. 7c) [33].

The results of our molecular docking studies revealed the potential inhibitory effect of Rif against SARS-CoV-2 main protease (3CL[pro]), since its docked binding energy (ΔG) was determined as -9.49 kcal·mol^{-1} and inhibition constant (Ki) as 110.13 nM (Table 2). It is very well known that an important effect on binding between a ligand and a receptor is triggered by hydrogen bond interactions. Thus, the interactions formed between Rif and chain A of 3CL[pro] during simulations were determined and illustrated in Fig. 7d. As can be seen, the drug molecule interacts with various amino acid residues in the 3CL[pro] binding pocket, as follows: Glu:166, Gln:189, Pro:168, Gly:170, Leu:167, 141, Phe:140, Met:165, Thr:190, Asn:142, His:163, Cys:145, Ser:144 (Fig. 7d and Table 2).

The results obtained by us regarding Rif capacity of inhibition against 3CL[pro] of SARS-CoV-2 are quite significant, demonstrating better therapeutic activity than other drugs already in use for COVID-19. For example, the drugs currently used in treating SARS-CoV-2 infected patients were initially investigated by similar molecular docking methods, resulting good inhibitory capacity against 3CL[pro] of SARS-CoV-2 virus, given by their binding energies: anti-HIV drugs – Ritonavir (-8.25 kcal·mol^{-1}), Lopinavir (-6.11 kcal·mol^{-1}), Abacavir (-7.77 kcal·mol^{-1}), Darunavir (-6.08 kcal·mol^{-1}); anti-H1N1 drug – Oseltamivir (-7.39 kcal·mol^{-1}); anti-malarial drugs – Chloroquine (-7.62 kcal·mol^{-1}), Azithromycin (-8.32 kcal·mol^{-1}), Hydroxychloroquine (-8.30 kcal·mol^{-1}) [18]. In contrast

Fig. 7 Schematic illustration of SARS-CoV-2 3CL^{pro} target protein (PDB: 6LU7) in complex with the drug Rif. (**a**) Molecular surface representation of the 3CL^{pro} homodimeric structure, showing chain A in cyan and chain B in purple. (**b**) Ribbon representation of chain A with the drug Rif locket inside the binding pocket, situated between domains I and II. Rif is presented in ball and stick representation, with different coloring for each atom type: carbon in grey, oxygen in red, and nitrogen in blue. (**c**) Enlarged visualization of Rif docking inside the binding pocket. The catalytic dyad composed of amino acid residues Cys 145 – His 41 is shown in purple. (**d**) Diagram of Rif and the surrounding amino acid residues present in 3CL^{pro} binding pocket. Hydrogen bond interactions (dashed red lines) and distances (Å)
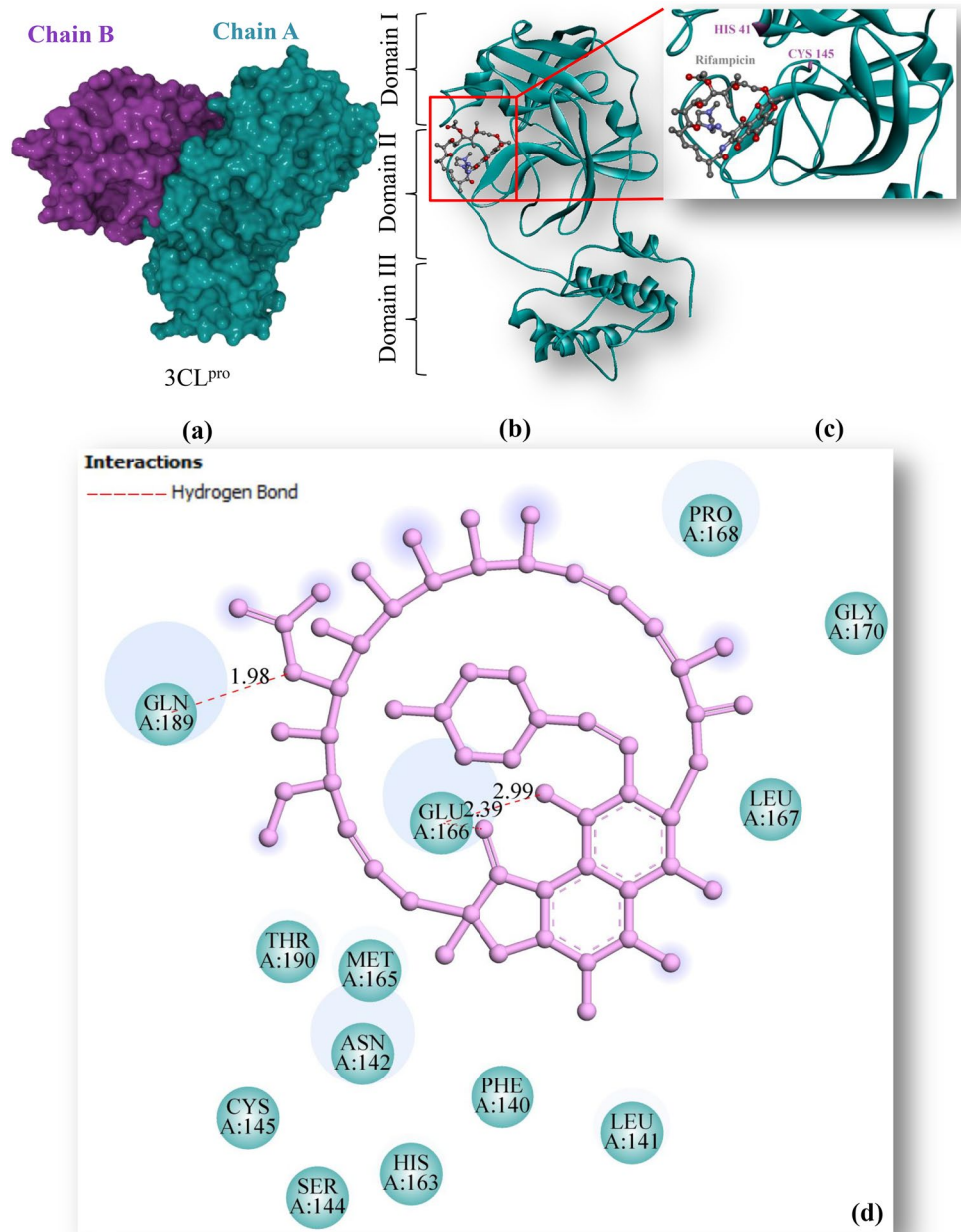
to these medications already used in hospitals around the World, Rif has shown superior inhibitory capacity given by its lower binding energy (-9.49 kcal·mol^{-1}), under the same investigation method, thus demonstrating greater efficiency. Moreover, it was mentioned before that SARS-CoV-2 binding to human cells is mediated by specific receptors, like ACE2 receptors present on airway epithelial cells and lung parenchyma. Therefore, inhibiting the renin-angiotensin system might be another possible strategy to eliminate SARS-CoV-2 infection. In this regard, Rif has been already reported to act as an anti-ACE2 agent [34, 35]. Furthermore, other records mention the successful using of Rif in treating patients infected with MERS-CoV,

which has a mortality rate higher than SARS-CoV-2 [29]. Also, a complicated case of a patient with COVID-19, which presented a pre-existing poly-infection with tuberculosis and HIV, was successfully treated with Rif [30].

In light of these valuable findings, we can conclude that Rif is a promising repurposed drug for the therapeutic management of current coronavirus pandemic, since it proved its inhibitory potential towards catalytic activity of 3CL^{pro} of SARS-CoV-2. Moreover, Rif is already approved by FDA for human use and its pharmacokinetics level is known, therefore no clinical trials are further required. This might speed up the development of efficient medications.

Table 2 Docking prediction of Rif against SARS-CoV-2 3CL^{pro}

Target protein	SARS-CoV-2 3CL^{pro}
Drug	Rifampicin
Binding energy (ΔG, kcal·mol^{-1})	-9.49
Inhibition constant (Ki, nM)	110.13
Amino acid residues involved in interaction	Glu:166, Gln:189, Pro:168, Gly:170, Leu:167, 141, Phe:140, Met:165, Thr:190, Asn:142, His:163, Cys:145, Ser:144
No. of hydrogen bond interactions (distance, Å)	3 (1.98, 2.39, 2.99)
Amino acid residue forming H bond with the drug	Gln:189, Glu:166

In addition to the Rif activity against main protease (3CL^{pro}) of SARS-CoV-2, Lap might also contribute to COVID-19 treatment. It is known that the molecular structures of clays are characterized by isomorphous substitution, which results in a charge deficiency on their surface. Their charged surface plays important role in clays affinity for other entities with charged surfaces, such as bacteria and microbes. In addition, their adhesivity, high absorption and low/no toxicity make them very important in biomedical field, as complexes and carriers for anticancer drugs or
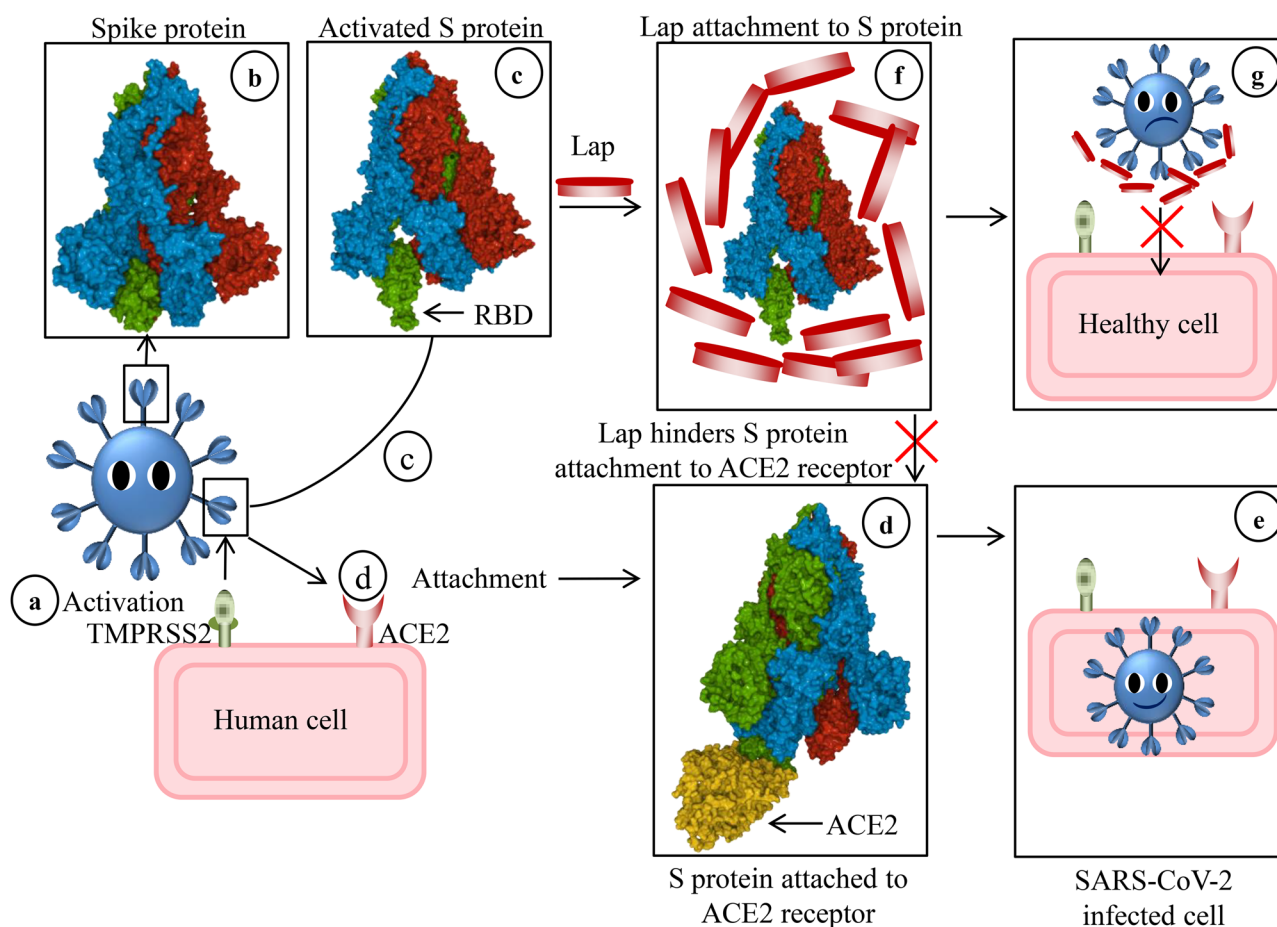

Fig. 8 Schematic representation of SARS-CoV-2 neutralization by clays which hinder its binding to ACE2 receptor and prohibit entering the human cell. (**a**) S protein priming by serine protease TMPRSS2, present on human cell. (**b**) Molecular surface representation of inactivated S protein. (**c**) Activated S protein with one RBD erect. (**d**) Activated S protein attachment to human cell ACE2 receptor. (**e**) Human cell infected with SARS-CoV-2. (**f**) Lap binds to S protein surface and hinders its attachment to ACE2 receptor. (**g**) SARS-CoV-2 engulfed by Lap can not enter human cell

transporters for sustained-release medicine [36–38]. There are several studies reporting the promising results obtained by using clays as antiviral materials, also against several coronaviruses and rotaviruses [12, 39]. Moreover, recently published in silico studies demonstrate high binding affinity/cohesiveness of clays with SARS-CoV-2 S proteins, capturing the virus prior to its binding with ACE2 receptor, suggesting that clays might act like pseudo-antibodies [10]. The schematic representation of clays neutralization mechanism by blocking S protein attachment to its target human cell receptor is presented in Fig. 8. As can be seen, S protein is primed by serine protease TMPRSS2, which activates it, and through its RBD attaches to ACE2 receptor on target cell. However, clays can closely interact by strong van der Waals attraction forces with RBD on surface glycoproteins of SARS-CoV-2, thus creating a higher cohesive energy density (CED) of clays/virus (S protein) molecular system than CED of virus (S protein)/human cell receptor (ACE2) molecular system. Thus, clays may act like antibodies, hindering virus attachment to target cells.

Conclusions

The present paper concludes that the obtained PVA/Lap hydrogel loaded with Rif might be a promising candidate as an efficient drug delivery system for COVID-19 treatment. Clays have been used in medical purposes for ages, including some coronaviruses treatment, due to their ability to attach to viral S proteins, prior their binding to human cell receptors. PVA is a well-known and highly employed polymer in pharmaceutical and medical applications, recommended by its excellent properties. Hydrogels obtained by freezing/thawing of PVA/Lap polymer solutions presented properties suitable for drug delivery systems (e.g., well defined porosity, mechanical stability, adequate swelling). Moreover, the adopted obtaining method (i.e., freezing/thawing) is bio-friendly and does not require the use of toxic cross-linkers. In vitro drug delivery tests showed that the drug Rif has a release profile/time dependent on hydrogels Lap content. In silico investigations of the drug capacity to inhibit 3CL^{pro} of SARS-CoV-2 were successful, showing a lower binding energy (i.e., -9.49 kcal·mol^{-1}). We recommend future in vitro and in vivo studies to confirm the above mentioned findings.

Declarations

References

1. Centers for Disease Control and Prevention (CDC) (2003) Revised U.S. surveillance case definition for severe acute respiratory syndrome (SARS) and update on SARS cases - United States and worldwide, December 2003. MMWR Morb Mortal Wkly Rep 52:1202–1206

2. Masters PS (2019) Coronavirus genomic RNA packaging. Virology 537:198–207. https://doi.org/10.1016/j.virol.2019.08.031

3. Harrison C (2020) Coronavirus puts drug repurposing on the fast track. Nat Biotechnol 38:379–381. https://doi.org/10.1038/d41587-020-00003-1

4. Li C-C, Wang X-J, Wang H-CR (2019) Repurposing host-based therapeutics to control coronavirus and influenza virus. Drug Discov Today 24:726–736. https://doi.org/10.1016/j.drudis.2019.01.018

5. Jiang S, Hillyer C, Du L (2020) Neutralizing antibodies against SARS-CoV-2 and other human coronaviruses. Trends Immunol 41:355–359. https://doi.org/10.1016/j.it.2020.03.007

6. Mohanty S, Harun AI Rashid M, Mridul M et al (2020) Application of artificial intelligence in COVID-19 drug repurposing. Diabetes Metab Syndr Clin Res Rev 14:1027–1031. https://doi.org/10.1016/j.dsx.2020.06.068

7. Li G, Clercq ED (2020) Therapeutic options for the 2019 novel coronavirus (2019-nCoV). Nat Rev Drug Discov 19:149–150. https://doi.org/10.1038/d41573-020-00016-0

8. Teodorescu M (2021) An overview of a year with COVID-19: What we know? Electron J Gen Med 18:em286. https://doi.org/10.29333/ejgm/9765

9. Gordon DE, Jang GM, Bouhaddou M et al (2020) A SARS-CoV-2-human protein-protein interaction map reveals drug targets and potential drug-repurposing. Nature 583:459–468. https://doi.org/10.1101/2020.03.22.002386

10. Abduljauwad SN, Habib T, Ahmed H-R (2020) Nano-clays as potential pseudo-antibodies for COVID-19. Nanoscale Res Lett 15:173. https://doi.org/10.1186/s11671-020-03403-z

11. Li W, Moore MJ, Vasilieva N et al (2003) Angiotensin-converting enzyme 2 is a functional receptor for the SARS coronavirus. Nature 426:450–454. https://doi.org/10.1038/nature02145

12. Clark KJ, Sarr AB, Grant PG et al (1998) In vitro studies on the use of clay, clay minerals and charcoal to adsorb bovine rotavirus and bovine coronavirus. Vet Microbiol 63:137–146. https://doi.org/10.1016/s0378-1135(98)00241-7

13. Morariu S, Teodorescu M (2020) Laponite® – A versatile component in hybrid materials for biomedical applications. Mem Sci Sect Romanian Acad 43:141–155

14. Teodorescu M, Bercea M, Morariu S (2018) Biomaterials of poly(vinyl alcohol) and natural polymers. Polym Rev 58:247–287. https://doi.org/10.1080/15583724.2017.1403928

15. Teodorescu M, Bercea M, Morariu S (2019) Biomaterials of PVA and PVP in medical and pharmaceutical applications: Perspectives and challenges. Biotechnol Adv 37:109–131. https://doi.org/10.1016/j.biotechadv.2018.11.008

16. Morariu S, Bercea M, Brunchi C-E (2018) Influence of Laponite RD on the properties of poly(vinyl alcohol) hydrogels. J Appl Polym Sci 135:46661. https://doi.org/10.1002/app.46661

17. Morariu S, Bercea M, Gradinaru LM et al (2020) Versatile poly(vinyl alcohol)/clay physical hydrogels with tailorable structure as potential candidates for wound healing applications. Mater Sci Eng C 109:110395. https://doi.org/10.1016/j.msec.2019.110395

18. Mamidala E, Davella R, Gurrapu S, Shivakrishna P (2021) In silico identification of clinically approved medicines against the main protease of SARS-CoV-2 – A causative agent of COVID-19. Int J Life Sci Pharma Res 11:107–122. https://doi.org/10.22376/ijpbs/lpr.2021.11.1.L107-122

19. Gupta A, Zhou H-X (2020) Profiling SARS-CoV-2 main protease (MPRO) binding to repurposed drugs using molecular dynamics simulations in classical and neural network-trained force fields. ACS Comb Sci 22:826–832. https://doi.org/10.1021/acscombsci.0c00140

20. Soni H, Gautam V, Sharma S, Malik J (2020) Rifampicin as potent inhibitor of COVID - 19 main protease: In-silico docking approach. Saudi J Med Pharm Sci 6:588–593. https://doi.org/10.36348/sjmps.2020.v06i09.001

21. Pathak Y, Mishra A, Tripathi V (2020) Rifampicin may be repurposed for COVID-19 treatment: Insights from an in-silico study. In: Res. Sq. Prepr. https://www.researchsquare.com. Accessed 19 Apr 2021

22. Brandrup J, Immergut EH, Grulke EA (2003) Polymer Handbook, 4th edn. Wiley

23. Jin Z, Du X, Xu Y et al (2020) Structure of Mpro from SARS-CoV-2 and discovery of its inhibitors. Nature 582:289–293. https://doi.org/10.1038/s41586-020-2223-y

24. Mezger TG (2006) The Rheology Handbook: For Users of Rotational and Oscillatory Rheometers. Vincentz Network GmbH & Co KG

25. Wilhelm M, Reinheimer P, Ortseifer M (1999) High sensitivity Fourier-transform rheology. Rheol Acta 38:349–356. https://doi.org/10.1007/s003970050185

26. Sollich P, Lequeux F, Hébraud P, Cates ME (1997) Rheology of Soft Glassy Materials. Phys Rev Lett 78:2020–2023. https://doi.org/10.1103/PhysRevLett.78.2020

27. Korsmeyer RW, Gurny R, Doelker E et al (1983) Mechanisms of solute release from porous hydrophilic polymers. Int J Pharm 15:25–35. https://doi.org/10.1016/0378-5173(83)90064-9

28. Rifampicin. https://go.drugbank.com/drugs/DB01045. Accessed 21 Apr 2021

29. Bleibtreu A, Jaureguiberry S, Houhou N et al (2018) Clinical management of respiratory syndrome in patients hospitalized for suspected Middle East respiratory syndrome coronavirus infection in the Paris area from 2013 to 2016. BMC Infect Dis 18:331. https://doi.org/10.1186/s12879-018-3223-5

30. Bouaré F, Laghmari M, Etouche FN, et al (2020) Unusual association of COVID-19, pulmonary tuberculosis and human immunodeficiency virus, having progressed favorably under treatment with chloroquine and rifampin. Pan Afr Med J 35:110. https://doi.org/10.11604/pamj.supp.2020.35.2.24952

31. Agrawal S, Panchagnula R (2005) Implication of biopharmaceutics and pharmacokinetics of rifampicin in variable bioavailability from solid oral dosage forms. Biopharm Drug Dispos 26:321–334. https://doi.org/10.1002/bdd.464

32. Tran PHL, Tran TTD (2021) Clay-based Formulations for Bioavailability Enhancement of Poorly Water-soluble Drugs. Curr Drug Metab. https://doi.org/10.2174/1389200222666210609170423

33. Jaskolski M, Dauter Z, Shabalin IG et al (2021) Crystallographic models of SARS-CoV-2 3CLpro: in-depth assessment of structure quality and validation. IUCrJ 8:238–256. https://doi.org/10.1107/S2052252521001159

34. Oroojalian F, Haghbin A, Baradaran B et al (2020) Novel insights into the treatment of SARS-CoV-2 infection: An overview of current clinical trials. Int J Biol Macromol 165:18–43. https://doi.org/10.1016/j.ijbiomac.2020.09.204

35. Abraham HMA, White CM, White WB (2015) The comparative efficacy and safety of the angiotensin receptor blockers in the management of hypertension and other cardiovascular diseases. Drug Saf 38:33–54. https://doi.org/10.1007/s40264-014-0239-7

36. Gianni E, Avgoustakis K, Papoulis D (2020) Kaolinite group minerals: Applications in cancer diagnosis and treatment. Eur J Pharm Biopharm 154:359–376. https://doi.org/10.1016/j.ejpb.2020.07.030

37. Pereira I, Saleh M, Nunes C et al (2021) Preclinical developments of natural-occurring halloysite clay nanotubes in cancer therapeutics. Adv Colloid Interface Sci 291:102406. https://doi.org/10.1016/j.cis.2021.102406

38. Tomás H, Alves CS, Rodrigues J (2018) Laponite®: A key nanoplatform for biomedical applications? Nanomedicine Nanotechnol Biol Med 14:2407–2420. https://doi.org/10.1016/j.nano.2017.04.016

39. Droy-Lefaix MT, Tateo F (2006) Chapter 11.6 Clays and Clay Minerals as Drugs. In: Bergaya F, Theng BKG, Lagaly G (eds) Developments in Clay Science. Elsevier, pp 743–752